frontiers | Frontiers in Earth Science

ORIGINAL RESEARCH
published: 14 April 2022
doi: 10.3389/feart.2022.863829

Asian Summer Monsoon Changes Inferred From a Stalagmite $\delta^{18}O$ Record in Central China During the Last Glacial Period

*Qingmin Chen[1†], Xing Cheng[1,2†], Yanjun Cai[2,3], Qianzhou Luo[4], Junliang Zhang[5], Li Tang[5], Yi Hu[5], Juangang Ren[6], Peng Wang[5], Yan Wang[5], Yu Zhang[5], Gang Xue[7], Jie Zhou[2], Hai Cheng[3,8], R. Lawrence Edwards[8] and Zenglin Hong[9,10,11]**

[1]Shaanxi Experimental Center of Geological Survey, Shaanxi Institute of Geological Survey, Xi'an, China, [2]State Key Laboratory of Loess and Quaternary Geology, Institute of Earth Environment, Chinese Academy of Science, Xi'an, China, [3]Institute of Global Environmental Change, Xi'an Jiaotong University, Xi'an, China, [4]Shaanxi Hygrogeology Engineering Geology and Environment Geology Survey Center, Shaanxi Institute of Geological Survey, Xi'an, China, [5]Shaanxi Mineral Resources and Geological Survey, Shaanxi Institute of Geological Survey, Xi'an, China, [6]Shaanxi Geological Science and Technology Center, Shaanxi Institute of Geological Survey, Xi'an, China, [7]State Key Laboratory of Continental Dynamics, Department of Geology, Northwest University, Xi'an, China, [8]Department of Earth Sciences, University of Minnesota, Minneapolis, MN, United States, [9]Shaanxi Institute of Geological Survey, Xi'an, China, [10]Research Center of Intelligent Geological Survey, Northwestern Polytechnical University, Xi'an, China, [11]Key Laboratory of Mine Geological Hazards Mechanism and Control, Ministry of Natural Resources, Xi'an, China

OPEN ACCESS

Edited by:
Yu Li,
Lanzhou University, China

Reviewed by:
Selvaraj Kandasamy,
Xiamen University, China
Amzad Hussain Laskar,
Physical Research Laboratory, India

***Correspondence:**
Zenglin Hong
lhqhzl@163.com

†These authors have contributed equally to this work and share first authorship

Specialty section:
This article was submitted to Quaternary Science, Geomorphology and Paleoenvironment, a section of the journal Frontiers in Earth Science

Received: *27 January 2022*
Accepted: *16 March 2022*
Published: *14 April 2022*

Citation:
Chen Q, Cheng X, Cai Y, Luo Q, Zhang J, Tang L, Hu Y, Ren J, Wang P, Wang Y, Zhang Y, Xue G, Zhou J, Cheng H, Edwards RL and Hong Z (2022) Asian Summer Monsoon Changes Inferred From a Stalagmite $\delta^{18}O$ Record in Central China During the Last Glacial Period. Front. Earth Sci. 10:863829. doi: 10.3389/feart.2022.863829

The reconstruction of Asian summer monsoon (ASM) changes during the last glacial period is of great significance for better understanding monsoon dynamics. The phase relationship between the Indian summer monsoon (ISM) and East Asian summer monsoon (EASM) subsystems on different timescales is still unclear. The comparative analysis of speleothem records in the ISM region, EASM region, and central China helps to clarify the relationship between the ISM and EASM. Based on the well-dated isotope records of stalagmite DDH-B15 from the Didonghe (DDH) Cave in Hanzhong, Shaanxi, we reconstructed ASM changes during the past 34–13 thousand years before the present (kyr BP). The small average error (61 years) of 18 uranium-series ages enables a precise comparison of the stalagmite $\delta^{18}O$ record with other well-dated records from the orbital to the millennial timescales. The $\delta^{18}O$ signal of the DDH-B15 stalagmite is controlled by changes of the low latitude northern hemisphere summer insolation (NHSI) on the orbital timescale. It records cold Heinrich Stadial (HS) and Dansgaard–Oeschger (DO) cycles which are originated from the northern high latitude on the millennial time scale. The $\delta^{18}O$ changes of stalagmites from the three regions are similar on the millennial and centennial timescales. But on the orbital-suborbital timescale, stalagmite $\delta^{18}O$ changes during the last glacial cycle have different characteristics. The stalagmite $\delta^{18}O$ values in eastern China became gradually negative, and the stalagmite $\delta^{18}O$ values in the Indian monsoon domain showed a increasing trend, but the stalagmite $\delta^{18}O$ values in Central China adopted an intermediate state between the EASM and ISM. Then we argued that the $\delta^{18}O$ value of stalagmites in Central China is a mixed signal of the ISM and EASM, which indicates a change of the water vapor source as an important influence on the Chinese stalagmite $\delta^{18}O$ record.

Keywords: speleothem, last glacial, Indian summer monsoon, East Asian summer monsoon, time scales, Chinese stalagmite $\delta^{18}O$

1 INTRODUCTION

The last glacial period is the most recent ice age of the Quaternary. Its internal climate exhibits huge fluctuations on orbital to millennial timescales (Johnsen et al., 1992; Rasmussen et al., 2014). A series of abrupt climate variations are observed on a millennial timescale, such as Heinrich Stadial (HS) and Dansgaard–Oeschger (DO) cycles. These events are characterized by rapid climate changes within decades and subsequent stability for hundreds to thousands of years (Heinrich, 1988; Alley et al., 1993; Dansgaard et al., 1993). This pattern of abrupt climate change has significance for future climate prediction (Corrick et al., 2020; Tierney et al., 2020).

The ASM includes two subsystems, the ISM and the EASM. The ASM brings abundant rainfall to the Asian continent during summer, whereas during winter, drier and cold conditions result from the Asian winter monsoon. This climate seasonality and its inter-annual variability affect the well-being of mankind in Asia which is a densely populated region (An, 2000; Wang et al., 2001a; Wang and Ding, 2008; Cheng et al., 2012; Wang et al., 2014). It is thus very important to figure out the rhythm of ASM changes. However, short-term modern meteorological observations limit our understanding of ASM dynamics, making it difficult to accurately predict long-term changes in the system. Reconstruction of the past evolutionary history of the ASM is of great significance to future monsoon predictions in the context of global warming. With the development of the uranium–thorium dating method (Edwards et al., 1987; Cheng et al., 2013), cave speleothems have become a favorable archive for tracking ASM changes through time on different timescales based on reconstructing oxygen isotope ($\delta^{18}O$) records (Wang et al., 2001b; Yuan et al., 2004; Cheng et al., 2016).

For example, on the glacial–interglacial timescale, dramatical sea level changes would have an important impact on the water vapor transport distance, resulting in stalagmite $\delta^{18}O$ in the ISM region that follow glacial–interglacial cycles, while speleothem $\delta^{18}O$ records in eastern coastal areas show smaller differences between glacial and interglacial periods, offsetting the ice volume cycle (Cai et al., 2015; Xue et al., 2019). On the precessional and millennial timescales, the signals of stalagmite $\delta^{18}O$ in the ASM region are more consistent (Zhang et al., 2021), which roughly reflects well-integrated precipitation on the Asian continent (Cheng et al., 2016; Cheng et al., 2021), or large-scale monsoon circulation, and/or the meridional migration of monsoon circulation (Hu et al., 2019). On the centennial–decadal–interannual timescales, stalagmite $\delta^{18}O$ is likely to represent changes in monsoon circulation, affected by the "circulation effect" (Tan, 2014), which is closely related to ENSO (Lu et al., 2021) or the position of the subtropical high (Zhao et al., 2019), and cannot be explained as changes in local rainfall. However, some stalagmites $\delta^{18}O$ can be used for reconstruction of local rainfall on the decadal-centennial timescales, with corrections using instrumental climate data (Tan et al., 2009; Tan et al., 2018).

It is also worth noting that the paleoclimate significance of speleothem (stalagmite) $\delta^{18}O$ requires a distinction on timescales and space scales. Stalagmite $\delta^{18}O$ records from the Hulu Cave in the EASM region reveal that the EASM experiences significant fluctuations on a millennial timescale and is coupled with climate changes in the northern high latitudes (Wang et al., 2001b). This finding has been subsequently supported by a large number of $\delta^{18}O$ records of Asian speleothems (Cai et al., 2006; Chen et al., 2016; Kathayat et al., 2016). Recent comparative studies on stalagmites across the globe with ice core records from Greenland also show abrupt climatic events in the ISM region, EASM region, and the South American monsoon region that responded synchronously or with lag times within the reported dating errors to climate changes in northern latitudes (Corrick et al., 2020). In addition, on the precessional timescale, the $\delta^{18}O$ value of stalagmites in the ISM and Central/eastern China changes in phase, and 23 kyr (and 19 kyr) precessional cycles are the main signals (Cai et al., 2015; Kathayat et al., 2016; Liu et al., 2020). On the glacial–interglacial timescale, most stalagmite $\delta^{18}O$ records in China lack an obvious 100 kyr cycle (Wang et al., 2008; Cheng et al., 2016), but monsoon proxies from the Chinese Loess Plateau do possess that cycle (Ding et al., 1995; Guo et al., 2000). Recent stalagmite $\delta^{18}O$ studies in the ISM region show that the ISM has a significant glacial–interglacial cycle besides the precessional cycle (Cai et al., 2015; Liu et al., 2020). However, on the orbital timescale, what drives the difference between the ISM and the EASM is still controversial (Cai et al., 2015; Cheng et al., 2021).

From a spatial perspective, although most records could capture signals of precessional and millennial events, the differences in the Chinese stalagmite $\delta^{18}O$ records from different regions are becoming apparent with the increasing number of stalagmite records. Stalagmite $\delta^{18}O$ changes in southern and northern China are basically consistent on the millennial timescale (Wang et al., 2001b; Duan et al., 2016; Dong et al., 2018) and the precessional timescale (Cheng et al., 2016; Li et al., 2020). However, stalagmite $\delta^{18}O$ in southern China may have 100 kyr cycles but not in northern China (Liu et al., 2022), and as Zhang et al. (2022) argues, during the MIS 3, a distinct precessional cycle is found in stalagmite $\delta^{18}O$ of the Yangzi Cave (Wu et al., 2020) and Yongxing Cave (Chen et al., 2016) but not from the Hulu Cave (Wang et al., 2001b), which may be caused by the increased contribution from spring rainfall to the stalagmite $\delta^{18}O$ in southeast China, and there are regional differences in stalagmite $\delta^{18}O$ on the centennial timescale (Tan et al., 2009). During the Holocene, there are asynchronous changes of stalagmite $\delta^{18}O$ in different caves when the Holocene Optimum terminated, early in the low latitude and late in the higher latitude (Cai et al., 2010). Therefore, timescales and regional differences should be considered when interpreting stalagmite $\delta^{18}O$. To understand this aspect, it is important to compare stalagmites $\delta^{18}O$ recording different endmember signals (the ISM region and EASM region), as well as samples from the region affected by both monsoon regimes, and analyze how they vary on different timescales.

We analyzed the $\delta^{18}O$ signal in a U-Th dated speleothem from the DDH Cave located in the Shaanxi province to understand the variability of monsoon changes during the 34–13 kyr BP. The DDH Cave is located in the region influenced by the two

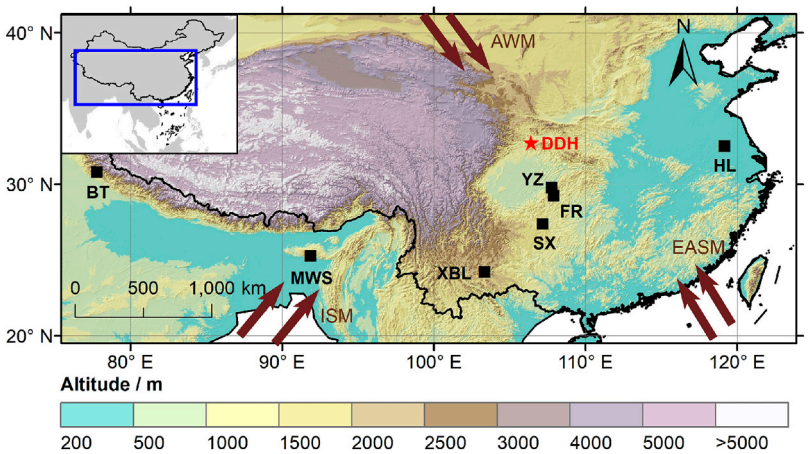

FIGURE 1 | Locations of speleothem records during the Last Glacial in the Asian monsoon region. (DDH, this study; YZ, Yangzi Cave, Wu et al., 2020; FR, Furon Cave, Li et al., 2021; SX, Sanxing Cave, Jiang et al., 2014; XBL, Xiaobailong Cave, Cai et al., 2015; NWS, Mawmluh Cave, Dutt et al., 2015; BT, Bitto Cave, Kathayat et al., 2016; HL, Hulu Cave, Wang et al., 2001b). The blown arrows indicate the Indian summer monsoon (ISM), the East Asian summer monsoon (EASM), and the Asian winter monsoon (AWM).

monsoon subsystems, recording valuable information of the complexity of the full ASM system during part of the last glacial cycle. We compared our results with other paleoclimate records on the orbital-suborbital time scales and identified the millennial timescale events in this period. We further analyzed the structure of those millennial events and discussed the variability of the monsoon during the LGM. Our study aimed to explore the controls of the ASM variability on the orbital to the millennial timescales and investigated the regional differences in speleothem $\delta^{18}O$ records.

2 CAVE LOCATION SETTINGS AND SAMPLE

Didonghe (DDH) Cave (32°44′14″N, 106°24′26″E, 1,262 m), located in Ningqiang County, Shaanxi province, China (**Figure 1**), is a karst cave of the Chanjiayan Tiankeng (sinkhole) system. The DDH Cave formed in the Permian Wujiaping limestone formation. It was overlain by the Permian Dalong shale and underlain by the Permian Wangpo shale (Luo et al., 2019). The stalagmite sample DDH-B15 was collected from the inner chamber of the cave, 2 km from the cave entrance. The inner chamber is closed, with high humidity and a stable sedimentation environment. Dripping water can be seen in the cave, and a large number of stalagmites, stalactites, flow stones, and other speleothems are developed there.

The study site is located in the southern Qinling Mountains, in Central China, where both the southwest ISM and EASM affect the climate (**Figure 1**). The climate is rainy and hot at the same time. In summer, southerly winds bring warm monsoon precipitation from low latitudes; in winter, northerly winds provide cold and dry air mass. According to meteorological monitoring records of the Ningqiang County Meteorological Station from 1957 to 2007, the average annual temperature in the Ningqiang area is 13°C, the average annual rainfall is 1,104 mm, and precipitation falls mainly during the summer monsoon season from June to September (Hu et al., 2010).

The sample used in this study has been briefly described in the works of Chen et al. (2020). The stalagmite was collected from the Yulong chamber at the deepest part of Cave B in the DDH Cave system. The speleothems were scattered on the ground during collection, possibly due to human activity or earthquake/cave collapse events. The DDH-B15 sample is 158 mm long, the bottom diameter is 64 mm at the widest part, and the top is about 30 mm in diameter. After cutting the stalagmite by using a diamond wire saw, the center of the sample was observed to be yellowish-brown, and the two sides were yellowish-white, with some cracks. In this study, we mainly considered the yellowish-brown central part to avoid the possible influence of pinch-out rocks on both sides on the climatic information. The growth axis of the stalagmite persists steadily, with only a few minor changes (**Figure 2A**). The stalagmite begins to gradually shift to the right about 40 mm from the top; the stalagmite grows vertically during the 40–120 mm portion, indicating a stable drip position; from 120 to 150 mm, the stalagmite growth shifts to the right likely due to a change in the karst seepage system.

3 METHODS

A dental burr was used to obtain 30–60 mg powder samples along the growth axis of DDH-B15. A total of 18 powdered subsamples were used to perform ^{230}Th-^{234}U-^{238}U age tests using a multi-cup inductively coupled plasma mass spectrometer (MC-ICP-MS) at the Isotope Laboratory, Xi'an Jiaotong University. We used a standard chemical pretreatment protocol (Edwards et al., 1987; Shen et al., 2002) before the test. A triple spike (^{229}Th-^{233}U-^{236}U) with known isotope concentrations was employed to determine the

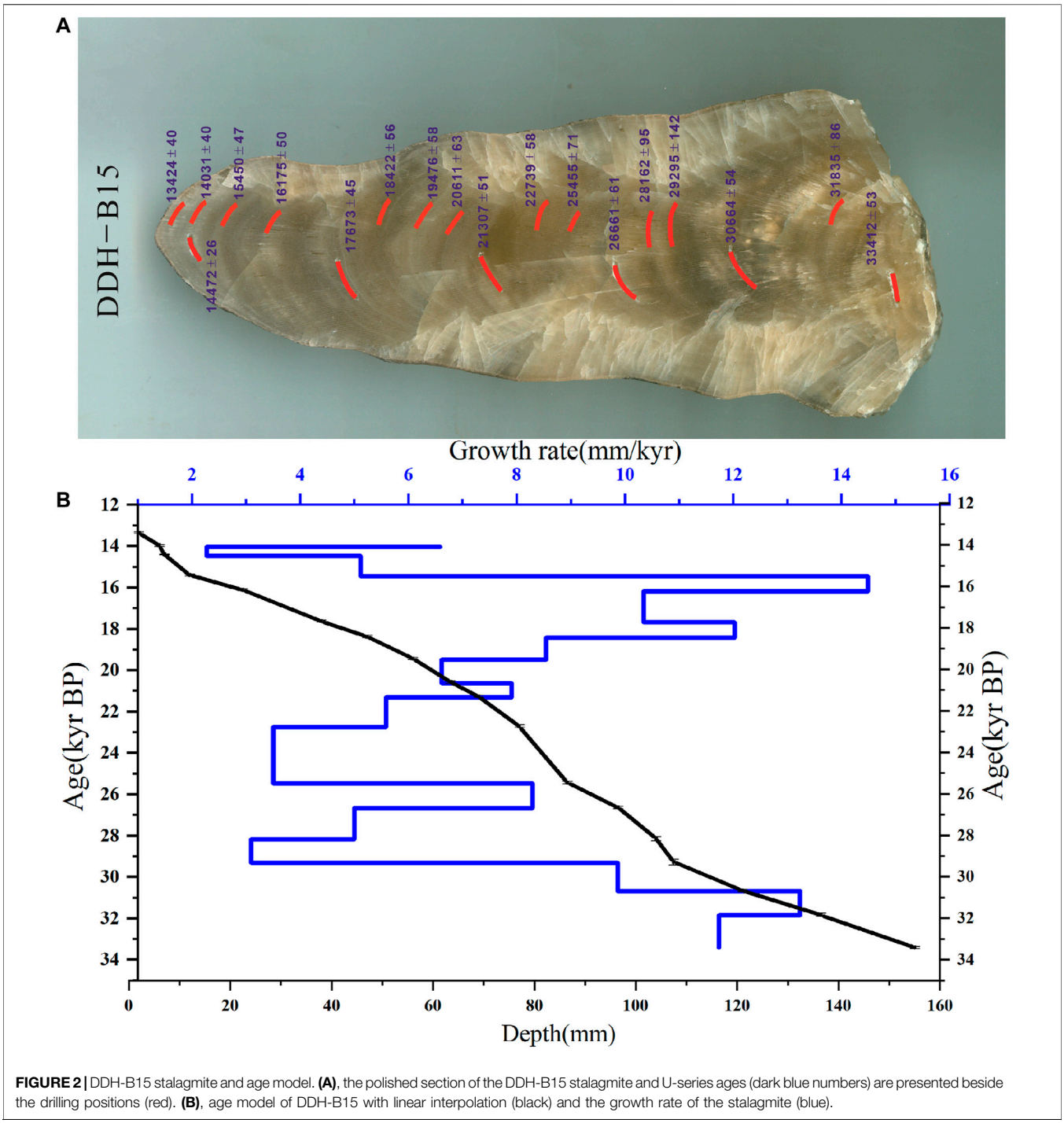

FIGURE 2 | DDH-B15 stalagmite and age model. **(A)**, the polished section of the DDH-B15 stalagmite and U-series ages (dark blue numbers) are presented beside the drilling positions (red). **(B)**, age model of DDH-B15 with linear interpolation (black) and the growth rate of the stalagmite (blue).

U-Th isotope ratio in the samples. We referred to Cheng et al. (2013) for a detailed description about the instrument, standardization, and half-lives. The U-Th ages are corrected according to $^{230}Th/^{232}Th = 4.4 \pm 2.2 \times 10^{-6}$ (atomic ratio) to deduct the influence of initial thorium, and all the dating errors are given at the 2σ level. Among them, the two top and bottom U-Th ages have been reported in Chen et al. (2020). In this study, 16 new U-Th ages have been tested and are listed as follows (**Table 1**).

Along the growth axis of DDH-B15, 322 sets of powder subsamples for carbon and oxygen isotope ($\delta^{13}C$ and $\delta^{18}O$) analyses were drilled by a dental burr at an even interval of 0.5 mm. All $\delta^{13}C$ and $\delta^{18}O$ measurements were carried out at the Institute of Earth Environment, Chinese Academy of Sciences, and the test instrument was an Isoprime100 gas source stable isotope ratio mass spectrometer equipped with a MultiPrep system. Generally, a laboratory internal standard TB1 is placed between every 15 samples to monitor the stability of the

TABLE 1 | ^{230}Th dating results of DDH-B15. The error is 2s error.

Sample	Depth	^{238}U		^{232}Th		^{230}Th/^{232}Th		δ^{234}U*		^{230}Th/^{238}U		^{230}Th age (yr)		^{230}Th age (yr)		$\delta^{234}U_{Initial}$**		^{230}Th age (yr BP)***	
Number	(mm)	(ppb)		(ppt)		(Atomic x10-6)		(Measured)		(Activity)		(Uncorrected)		(Corrected)		(Corrected)		(Corrected)	
DDH-B15-B1	**2**	775.6	±1.1	1,654	±34	4,926	±101	4,386.2	±4.7	0.6370	±0.0017	13504	±40	**13493**	**±40**	4,556	±5	**13424**	**±40**
DDH-B15-B2	**6**	757.4	±1.2	450	±10	18691	±427	4,465.5	±5.4	0.6738	±0.0017	14103	±40	**14100**	**±40**	4,647	±6	**14031**	**±40**
DDH-B15-T	**7**	1,141.1	±1.0	3917	±79	3302	±66	4,411.5	±3.3	0.6875	±0.0009	14557	±22	**14539**	**±26**	4,596	±3	**14472**	**±26**
DDH-B15-B3	**12**	1,056.0	±1.7	101	±6	122571	±6896	4,290.5	±5.3	0.7142	±0.0019	15519	±47	**15519**	**±47**	4,483	±6	**15450**	**±47**
DDH-B15-B4	**22.5**	1,225.0	±2.3	114	±5	134915	±5,997	4,411.0	±5.9	0.7628	±0.0021	16244	±50	**16244**	**±50**	4,618	±6	**16175**	**±50**
DDH-B15-1	**38**	1,131.6	±1.7	421	±10	36913	±863	4,442.5	±4.6	0.8337	±0.0018	17742	±45	**17740**	**±45**	4,671	±5	**17673**	**±45**
DDH-B15-B5	**47**	876.6	±1.6	68	±4	187333	±12408	4,503.1	±5.9	0.8765	±0.0023	18491	±56	**18491**	**±56**	4,744	±6	**18422**	**±56**
DDH-B15-B6	**56**	1,010.0	±1.6	74	±6	197300	±15891	4,260.3	±5.2	0.8822	±0.0023	19545	±58	**19545**	**±58**	4,502	±6	**19476**	**±58**
DDH-B15-B7	**63.5**	803.8	±1.3	135	±6	90949	±4,356	4,242.4	±5.0	0.9268	±0.0025	20681	±63	**20680**	**±63**	4,497	±5	**20611**	**±63**
DDH-B15-2	**69**	988.7	±1.2	395	±9	39039	±884	4,184.8	±3.9	0.9452	±0.0020	21377	±51	**21374**	**±51**	4,445	±4	**21307**	**±51**
DDH-B15-B8	**77**	975.5	±1.4	105	±5	152777	±6877	4,174.0	±4.8	1.0016	±0.0022	22809	±58	**22808**	**±58**	4,452	±5	**22739**	**±58**
DDH-B15-B9	**86.5**	1,008.5	±1.7	247	±6	77843	±1886	4,385.5	±5.7	1.1564	±0.0027	25525	±71	**25524**	**±71**	4,713	±6	**25455**	**±71**
DDH-B15-3	**96.5**	1,004.3	±1.5	289	±7	69036	±1,564	4,374.0	±5.1	1.2035	±0.0022	26729	±61	**26728**	**±61**	4,717	±6	**26661**	**±61**
DDH-B15-A1	**104**	1,245.8	±2.5	113	±8	224468	±15623	4,265.0	±6.9	1.2390	±0.0034	28231	±95	**28230**	**±95**	4,619	±8	**28162**	**±95**
DDH-B15-A2	**107.5**	1,043.1	±2.1	160	±12	137152	±9939	4,235.2	±7.4	1.2765	±0.0053	29363	±142	**29363**	**±142**	4,601	±8	**29295**	**±142**
DDH-B15-4	**121**	969.8	±0.9	91	±4	225550	±8951	4,065.7	±3.4	1.2866	±0.0018	30732	±54	**30731**	**±54**	4,434	±4	**30664**	**±54**
DDH-B15-B10	**136.5**	976.1	±1.4	84	±3	258162	±9245	4,115.7	±5.1	1.3437	±0.0029	31905	±86	**31904**	**±86**	4,503	±6	**31835**	**±86**
DDH-B15-B	**155**	1,151.3	±1.1	838	±17	31973	±649	4,149.0	±3.6	1.4121	±0.0017	33483	±53	**33479**	**±53**	4,560	±4	**33412**	**±53**

U decay constants: $\lambda_{238} = 1.55125 \times 10^{-10}$ (Jaffey et al., 1971) and $\lambda_{234} = 2.82206 \times 10^{-6}$ (Cheng et al., 2013). Th decay constant: $\lambda_{230} = 9.1705 \times 10^{-6}$ (Cheng et al., 2013).$\delta^{234}U = ([^{234}U/^{238}U]activity–1)\times1{,}000$. **$\delta^{234}U_{Initial}$ was calculated based on ^{230}Th age (T), i.e., $\delta^{234}U_{Initial} = \delta^{234}U_{measured} \times e^{\lambda 234 \times T}$. Corrected ^{230}Th ages assume the initial $^{230}Th/^{232}Th$ atomic ratio of $4.4 \pm 2.2 \times 10^{-6}$. These are the values for a material at secular equilibrium, with the bulk earth $^{232}Th/^{238}U$ value of 3.8. The errors are arbitrarily assumed to be 50%.***B.P. stands for "before present" where the "Present" is defined as the year 1950 A.D.*

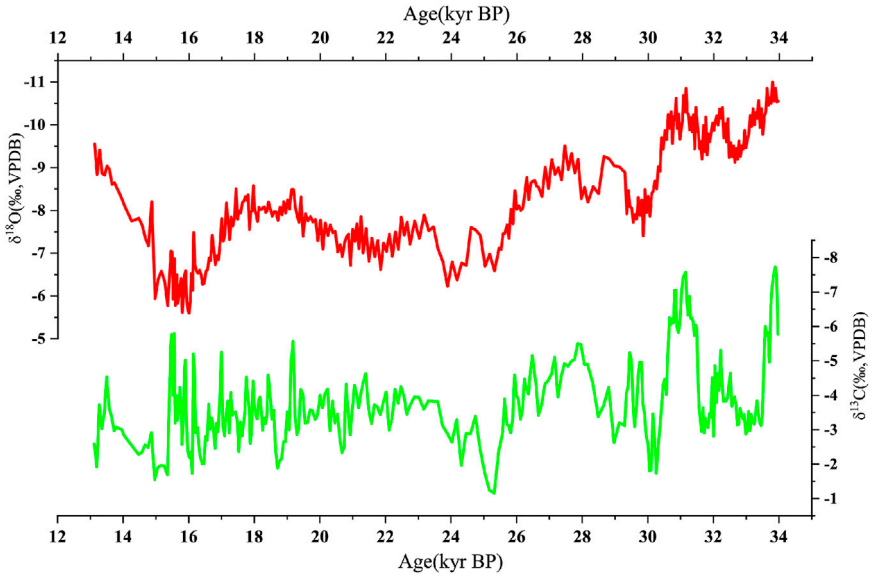

FIGURE 3 | DDH-B15 $\delta^{18}O$ (red) and $\delta^{13}C$ (green) time series.

instrument, and one sample out of every 10–20 samples is randomly selected to verify its repeatability. The $\delta^{13}C$ and $\delta^{18}O$ test results are given according to the VPDB standard. The precision for $\delta^{18}O$ and $\delta^{13}C$ measurements of standard materials is better than 0.15‰ and 0.12‰ (2σ).

4 RESULTS

4.1 U-Th Age Model

Including the top and bottom ages (14.5 kyr BP at 7 mm and 33.3 kyr BP at 155 mm) reported by Chen et al. (2020), 18 U-Th high-precision ages were obtained (**Table 1**). The uranium concentration of the DDH-B15 stalagmite ranges from 757.4 to 1,245.8 parts per billion (ppb), with an average of 1,007.8 ppb, which is a relatively high uranium content for calcite stalagmites. The content of Th depends mainly on the ^{232}Th content. The range of ^{232}Th is 74-3917 parts per trillion (ppt), and the average value is 514ppt. The range of $^{230}Th/^{232}Th$ is 3302-258162 (atomic ratio), and its average value is 111828. Compared with the initial $^{230}Th/^{232}Th$ value of 4.4 ± 2.2 (atomic ratio), the correction error caused by the initial thorium does not exceed 1‰, which can be ignored. $\delta^{234}U_{Initial}$ varies between 4,434‰ and 4,744‰, with an average value of 4,575‰. The obtained 18 U-Th ages are between 33.4 kyr BP and 13.4 kyr BP, with errors between 26 and 142 years, and the average error being 61 years (the average relative error is 2.76‰). All ages are in stratigraphic order, and linear interpolation was used to establish a chronological model. The age model results show that the growth period of the stalagmite is from 33.97 to 13.12 kyr BP (**Figure 2B**). The growth rate of DDH-B15 is relatively stable (2.3–14.5 mm/kyr), and the average growth rate is 7.89 mm/kyr. The stalagmite grew fast during 34–29 kyr BP and 22–16 kyr BP but slowly in other periods (**Figure 2B**).

4.2 DDH-B15 $\delta^{18}O$ and $\delta^{13}C$ Time Series

Using the chronological scale established earlier, a $\delta^{18}O$ time series was constructed for the DDH-B15 stalagmite (**Figure 3**). The average temporal resolution of $\delta^{18}O$ series is 64.8 years during 33.97–13.12 kyr BP, which can be used to study climate variability on centennial–millennial–suborbital timescales. DDH-B15 $\delta^{18}O$ values vary from −11‰ to −5.6‰, with an overall increasing trend from 34 kyr BP to 16 kyr BP, and rapidly shift to negative values after 15 kyr BP. The entire $\delta^{18}O$ sequence is interrupted by three significant positive events, roughly at 16 kyr BP, 24 kyr BP, and 29.5 kyr BP. In addition, among several significant positive events, the $\delta^{18}O$ values of 34–30 kyr BP, 29–26 kyr BP, and 21–17 kyr BP were relatively negative. Among them, the $\delta^{18}O$ values during the 34–30 kyr BP period is the most negative, which are ~5‰ more negative than the most positive value observed at 16 kyr BP. Furthermore, during 21–17 kyr BP, $\delta^{18}O$ series values grasp an obvious negative event, which is also reflected in records from other stalagmites in the ASM region (Wang et al., 2001b; Cai et al., 2010; Jiang et al., 2014).

DDH-B15 $\delta^{13}C$ values fluctuate between −7.73‰ and −1.16‰. While we observe a significant long-term increasing trend of $\delta^{18}O$, the $\delta^{13}C$ values show only a slight positive trend (**Figure 3**) on the orbital timescale. On the millennial timescale, $\delta^{13}C$ and $\delta^{18}O$ show similar characteristics at some excursions of enriched isotope events but also with some differences. For example, during 21–17 kyr BP, $\delta^{13}C$ does not have a significant depleted value as seen in $\delta^{18}O$; while during 17–15 kyr BP, $\delta^{13}C$ exhibits large fluctuations and tends to be negative but not positive. Subsequent to 15 kyr BP, the positive trend of $\delta^{13}C$ is gradually reestablished. However, during the period of 34–31 kyr BP, $\delta^{18}O$ only shows a modest (~1‰) oscillation, while $\delta^{13}C$ shifts up to 4.5‰. $\delta^{18}O$ has a long-term trend, with an overall variation range of about 5.5‰, while $\delta^{13}C$

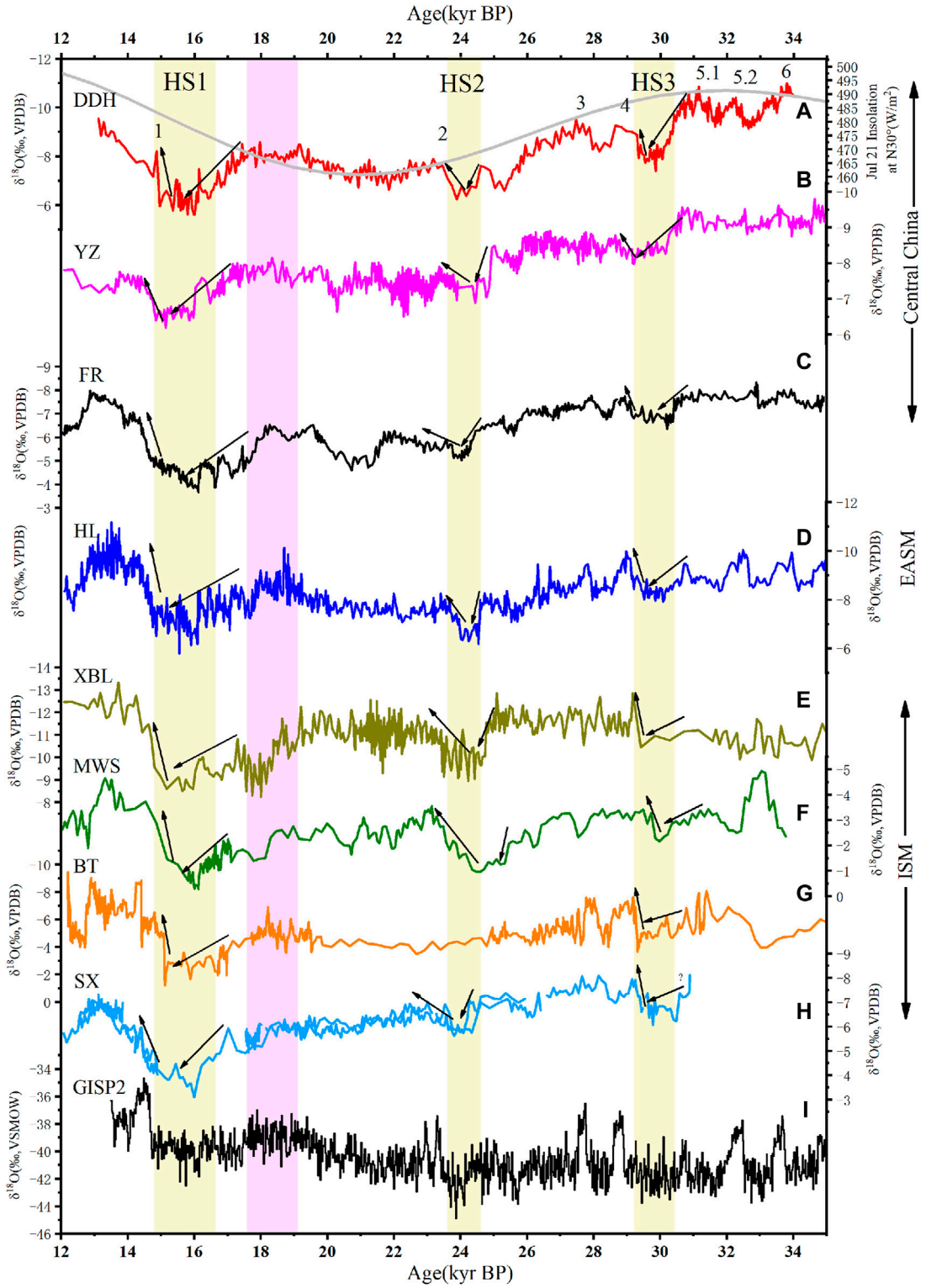

FIGURE 4 | Comparison of DDH speleothem $\delta^{18}O$ records (Central China) with other paleoclimate records (EASM and ISM regions). a, DDH Cave, this study; b, Yangzi Cave (Wu et al., 2020); c, Furon Cave (Li et al., 2021); d, Hulu Cave (Wang et al., 2001b);e, Xiaobailong Cave (Cai et al., 2015); f, Mawmluh Cave (Dutt et al., 2015); g, Bitto Cave (Kathayat et al., 2016);h, Sanxing Cave (Jiang et al., 2014); and k, Greenland ice core (Rasmussen et al., 2014). Shaded in pink are monsoon intensification events during the LGM, and the yellow bars are three HS events.

has no obvious trend on the suborbital timescale, and its millennial signal varies by as much as 6.5‰. This suggests that $\delta^{13}C$ is more sensitive to climate change than $\delta^{18}O$ on the millennial timescale.

5 DISCUSSION

5.1 Interpretation of Stalagmite $\delta^{18}O$ and $\delta^{13}C$ of the DDH Cave

Before interpreting the climatic significance of stalagmite $\delta^{18}O$ of the DDH Cave, it is necessary to judge whether the stalagmite calcite was deposited under an isotopic equilibrium. Recently, the most widely used equilibrium fractionation test is the replication of $\delta^{18}O$ records from different stalagmites in the same cave or from different caves in the same climate region (Dorale et al., 1998; Wang et al., 2001b; Dorale and Liu 2009; Li et al., 2019). Comparing the $\delta^{18}O$ records of the DDH stalagmite with other contemporaneous stalagmite records in the ASM region, it is observed that the DDH stalagmite $\delta^{18}O$ record is consistent with that of the Hulu Cave (Wang et al., 2001b) and Yangzi Cave (Wu et al., 2020) and that major millennial timescale events are well recorded, such as HS1 at 16 kyr BP, HS2 at 24 kyr BP, HS3 at 29.5 kyr BP, and seven DO events (**Figure 4**). The correlation coefficient between the DDH stalagmite $\delta^{18}O$ and Hulu stalagmite $\delta^{18}O$ is 0.76 ($N = 349$ and $p < 0.001$), and the correlation coefficient of the Yangzi stalagmite $\delta^{18}O$ is 0.83 ($N = 349$ and $p < 0.001$). Therefore, we have reason to assume that the DDH-B15 stalagmite was deposited under (near-)equilibrium fractionation conditions, and the influence of kinetic fractionation is negligible.

The stalagmite $\delta^{18}O$ is mainly controlled by the cave temperature and drip $\delta^{18}O$ changes (Lachniet, 2009). The DDH-B15 $\delta^{18}O$ variation is 5.5‰. The $\delta^{18}O$ fractionation coefficient (−0.23‰/°C, O'Neil et al., 1969) caused by the temperature is very small. The 34–13 kyr BP belongs to the MIS3-2 stage, when the global average temperature did not change in the region by more than 4°C (Peterse et al., 2014). Indeed, an 8°C change between glacial and interglacial cycles in the Loess Plateau (Peterse et al., 2014) only implies a maximum temperature contribution around 1.8‰. Therefore, we can interpret the DDH-B15 stalagmite $\delta^{18}O$ values as indicators of precipitation $\delta^{18}O$.

The climatic significance of the Chinese stalagmite $\delta^{18}O$ is controversial (Maher, 2008; Pausata et al., 2011; Liu et al., 2020). In the ASM region, especially in eastern China, the stalagmite $\delta^{18}O$ values are variably affected by many factors. Early studies had shown that the amount of rainfall was not significantly negatively correlated with $\delta^{18}O$ values (Wang et al., 2001b). At the same time, Cai et al. (2001) had proposed that different moisture sources may affect stalagmite $\delta^{18}O$ values. Wang et al. (2001a) used the ratio of summer/winter rainfall to explain the $\delta^{18}O$ of stalagmites and introduced the concept of "monsoon intensity." Cheng et al. (2009, 2016, 2021) followed and extended the concept of "monsoon intensity" and believed that the lower stalagmite $\delta^{18}O$ mainly represented the higher spatially integrated monsoon rainfall between the tropical monsoon sources and reflected "wind" characteristics of the monsoon. Yuan et al. (2004) believed that the stalagmite $\delta^{18}O$ record was dominated by Rayleigh distillation processes associated with the water vapor transport, that is, the "rainout effect" or "continental effect". Subsequent work on paleoclimate records and simulations also basically supported these two interpretations (Hu et al., 2008; Pausata et al., 2011; Liu et al., 2014; Hu et al., 2019). The contribution of the rainout effect and the proportion of summer rainfall remain uncertain (Orland et al., 2009; Liang et al., 2020). Chinese stalagmite $\delta^{18}O$ records are very consistent on precessional-millennial timescales (Wang et al., 2001b; Cheng et al., 2009). At present, $\delta^{18}O$ is still the most effective stalagmite paleoclimate proxy. Most researchers approve that $\delta^{18}O$ can be an indicator of monsoon rainfall in northern China or the Asian continent.

The DDH cave is located on the southern slope of the Qinling Mountains, about 500 km away from the Sanbao Cave and Linzhu Cave (Cheng et al., 2016). The DDH stalagmite $\delta^{18}O$ is very similar to the compositive stalagmite $\delta^{18}O$-based records from the Sanbao–Dongge–Hulu–Linzhu Cave (**Figure 4**), and the long-scale changes of the DDH stalagmite $\delta^{18}O$ are consistent with summer insolation changes in the northern hemisphere. Recent EASM reconstruction by the loess microcodium $\delta^{18}O$ presented an opportunity to reconcile the paradox between speleothems and loess, which showed that the dominated signal of the EASM was precession but the ice volume influenced the amplitude. The loess microcodium $\delta^{18}O$ consisted of speleothem $\delta^{18}O$ on precessional and millennial scales (Zhang et al., 2022). This also reveals that the speleothem $\delta^{18}O$ can be used as a monsoon tensity index. In addition, the stalagmite $\delta^{18}O$ in the Xianglong Cave, 20 km away from the DDH Cave, was consistent with the local rainfall on the decadal timescale (Tan et al., 2015, 2018). The DDH stalagmite $\delta^{18}O$ should show similar disciplinary. Considering the aforementioned data, the "monsoon intensity" concept is followed (Cheng et al., 2016); we argue that the $\delta^{18}O$ of the DDH stalagmite reflects monsoon intensity changes and integrated rainfall changes on a large spatial scale. When the stalagmite $\delta^{18}O$ is negative, the ASM rain belt is pushed northward, the rainfall in north China increases, and the rainfall in the south may be different (Cheng et al., 2016, 2019). On a shorter timescale, it is affected by local hydrology and climate. There may be some differences between the stalagmite $\delta^{18}O$ and rainfall index. $\delta^{13}C$ may represent changes of the local hydroclimate because when precipitation increases, the proportion of C_3 vegetation increases, vegetation coverage becomes larger, and the water–rock interaction (WRI) time becomes shorter, which will make $\delta^{13}C$ more negative (Dorale et al., 1992; Baker et al., 1997). The relationship between $\delta^{13}C$ and $\delta^{18}O$ on different timescales may represent the relationship between local precipitation and Asian monsoon intensity. They are not identical on the orbital scale but have certain similarities on the millennial scale (**Figure 4**). But stalagmite $\delta^{13}C$ is also affected by temperature, cave ventilation, prior calcite precipitation (PCP) process, atmospheric CO_2, and other factors (Fairchild et al., 2006; Genty et al., 2006). Therefore, it is necessary to further study

the DDH stalagmite $\delta^{13}C$ combined with other hydrological proxies, but it is not discussed here. In the following sections, we focused on the changes of our DDH stalagmite $\delta^{18}O$ on multiple timescales and regional differences.

5.2 Characteristics of Orbital-Suborbital and Abrupt Events Recorded by the DDH Stalagmite $\delta^{18}O$ During the Last Glacial

On the orbital-suborbital timescales, the $\delta^{18}O$ of the DDH stalagmite is consistent with other caves and is mainly controlled by summer insolation in the northern hemisphere (**Figure 4**). The overall trend of the DDH stalagmite $\delta^{18}O$ is similar to the Yangzi Cave (Wu et al., 2020) and the Hulu Cave (Wang et al., 2001b) stalagmite $\delta^{18}O$; however, during the period of 34–30 kyr BP, the Chinese cave records also showed some differences. The DDH $\delta^{18}O$ changes from a negative value to a positive value, while the Hulu Cave stalagmite $\delta^{18}O$ is relatively stable, with no significantly persistent positive trends during 34–18 kyr BP. In addition, the Hulu cave $\delta^{18}O$ values during the 19–17 kyr BP period are nearly as negative as those observed in the 34–30 kyr BP period (**Figure 4**). The stalagmite $\delta^{18}O$ values from the Xiaobailong Cave in Yunnan (Cai et al., 2015) were relatively stable or even gradually negative during the 34–20 kyr BP period. Mawmluh Cave (Dutt et al., 2015) and Bitto Cave (Kathayat et al., 2016) from the ISM region also share similar characteristics, which may be influenced by the low time resolution of the record, or be a characteristic in the ISM region. Therefore, further research is needed for verification. The significant negative $\delta^{18}O$ values of the DDH Cave and the Yangzi Cave during the 34–30 kyr BP period may be related to a stronger summer insolation. However, the Hulu Cave stalagmite $\delta^{18}O$ values are not closely related to insolation during this period.

On the millennial timescale, the DDH stalagmite $\delta^{18}O$ record shows seven warm DO cycles (**Figure 4A**). The DO1 event, which is the Bolling event, occurred at 15–14 kyr BP, DO2 occurred at 23.5–23 kyr BP, DO3 occurred at 28–27.5 kyr BP, DO4 occurred at 29.2–28.6 kyr BP, DO5.1 occurred at 31.5–30.5 kyr BP, DO5.2 occurred at 32.5–32 kyr BP, and DO6 occurred at 34–33.5 kyr BP. The seven DO events in our records are temporally consistent with the Greenland ice core, but there are some differences in the structure. The onsets of these DO warm events are not very rapid, which are similar to other stalagmites in the Asian monsoon region, but not as rapid as the warming shift recorded by the arctic ice core, which may be influenced by the climate of the southern hemisphere (Cai et al., 2006; Rohling et al., 2009). In addition, the DDH stalagmite $\delta^{18}O$ and other stalagmites $\delta^{18}O$ records from the ASM region also record three significant HS cold events on the millennial timescale (**Figure 4**). HS1 occurred at 17–15 kyr BP, HS2 occurred at 24.5–23.5 kyr BP, and HS3 occurred at 30.5–29.2 kyr BP. As described by Li et al. (2019), two phases of weak monsoon occurred in the Central China at the onset of the HS1 cold event. The stalagmite records in the ISM area also exhibit a two-phase structure (**Figure 4**). In addition, at the end of HS1, the DDH record and the Hulu Cave, Xiaobailong Cave, Sanxing Cave, and others also showed a two-stage process of monsoon enhancement. In general, this two-stage enhancement process can be regarded as a multi-cycle slow enhancement process. Four internal turbulent events at the onset of HS1 can be found in the Greenland ice core, Hulu Cave, and DDH records. The onset and termination of HS2 and HS3 events from high latitudes may also have multi-stage structures, but the performance is not obvious in DDH and other stalagmite records, which may be attributed to duration or time resolution limitations (**Figure 4**).

Comparing the DDH stalagmite $\delta^{18}O$ record with other stalagmite $\delta^{18}O$ records, it is found that the three HS events do not have exactly the same structural characteristics. Generally speaking, HS1 and HS3 events are characterized by slow entry and rapid termination. This mode has similar characteristics to the glacial–interglacial cycle, which may be related to the "binge-purge" dynamic mechanism of ice sheet evolution (MacAyeal, 1993), while HS2 and Holocene millennial events (such as 4.2 and 8.2 kyr) mainly enter quickly and terminate slowly (Liu et al., 2018). This implies that the HS1 and HS3 events of the glacial period are different from the Bond events of the interglacial period (Liu et al., 2018), and the structure of the HS2 event is different from the other two HS events.

Considering the aforementioned characteristics together, we found that precessional and millennial signals are the main portrait of the ASM, and low latitude summer insolation is the driving force of the ASM which is coupled with high-latitude climate changes on the millennial scale. However, there are some differences in the stalagmite $\delta^{18}O$ of different caves on the suborbital scale, and there are also some differences in the structure of different HS events.

5.3 Periodic Characteristics of DDH Stalagmite $\delta^{18}O$ Changes

In order to assess the dominant period of the DDH stalagmite $\delta^{18}O$, we first used REDFIT software (Schulz and Mudelsee, 2002) to analyze the $\delta^{18}O$ signal. It is found that the DDH stalagmite $\delta^{18}O$ has significant periods of 555, 206, and 142 years (**Figure 5**), consistent with the main periods observed in the Holocene Dongge Cave $\delta^{18}O$ record (Wang et al., 2005; Dykoski et al., 2005). These periodicities are close to significant periods (512, 206, and 148 years) of the $\triangle$14C record (Stuiver and Braziunas, 1993). Therefore, 555, 206, and 142 years are the main periods associated with solar activity. It is observed that 206 years is the Suess period of solar activity and 555 years may be the significant 500-year period of the ASM (Xu et al., 2019), Greenland temperature (Stuiver et al., 1995), and ENSO variability (Zhu et al., 2017). These periods support the idea that solar activities are responsible for changes of glacial ASM intensity.

For distinguishing the variability of the DDH stalagmite $\delta^{18}O$ on different timescales, the EEMD method (Wu and Huang, 2009) is employed to decompose it. At the same time, we also compared the variability of the stalagmite $\delta^{18}O$ from the ISM region and the EASM region on different timescales. The Hulu Cave and XBL Cave with high resolution $\delta^{18}O$ and an accurate age model are selected as representatives of the EASM and ISM. Interpolating the three records to a resolution of 30 years, we used

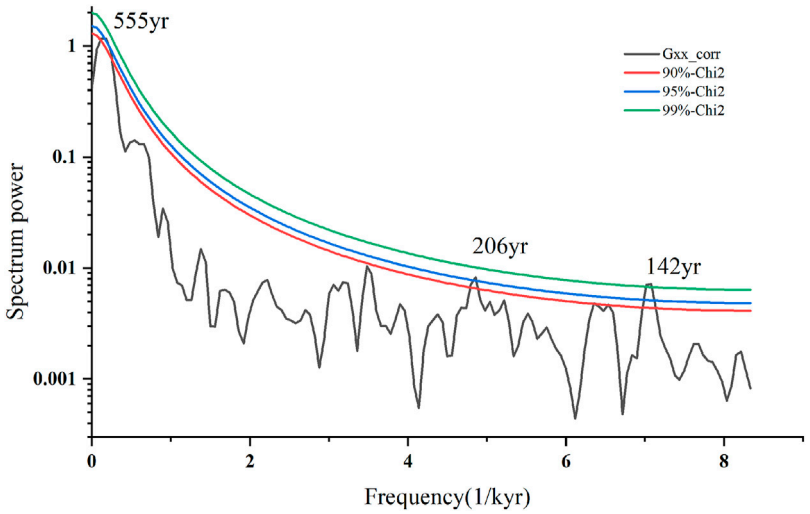

FIGURE 5 | Spectrum analysis of DDH $\delta^{18}O$.

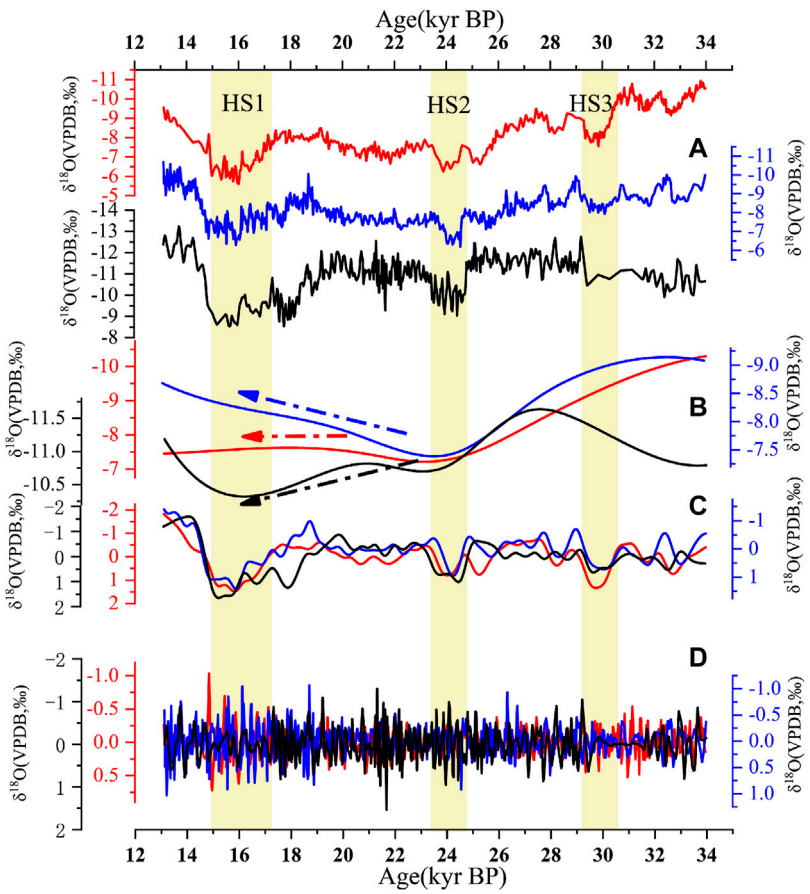

FIGURE 6 | a, Speleothem $\delta^{18}O$ of the DDH Cave (red, Central China), Hulu Cave (blue, EASM), and Xiaobailong Cave (black, ISM); b, IMF 7-9 component of the speleothem $\delta^{18}O$ in the DDH Cave, Hulu Cave, and Xiaobailong Cave, which are mainly the cycles of suborbital-orbital periods; c, IMF C4-6 component of speleothem $\delta^{18}O$ in the DDH Cave, Hulu Cave, and Xiaobailong Cave, which are mainly millennial cycles; d, IMF C1-3 component of the speleothem $\delta^{18}O$ in the DDH Cave, Hulu Cave, and Xiaobailong Cave, which are mainly centennial cycles.

the EEMD method to decompose the DDH stalagmite $\delta^{18}O$ into nine components, including the long trend. These nine components extend the period from orbital to suborbital, millennial, and centennial time scales (**Figure 6**). IMF C7-C9 (**Figure 6B**) are reconstructed to form a new component of the orbital-suborbital timescale, which should be dominated by precessional signals (Yuan et al., 2004; Wang et al., 2008); IMF C4-6 (**Figure 6C**) are reconstructed to form a millennial time scale component, including cycles of 5,000, 2000, and 1,000 years, which are consistent with the northern high latitude temperature changes (Bond et al., 1999; Wang et al., 2008); IMF C1-3 (**Figure 6D**) are reconstructed to obtain cycles below the millennial time scale, which are mainly on the centennial time scale, corresponding to 200- and 500-year cycles of solar activity.

On the three different timescales, the stalagmite $\delta^{18}O$ records of the three regions have similarities and differences. On the centennial (**Figure 6D**) and millennial (**Figure 6C**) timescales, stalagmite $\delta^{18}O$ changes in the three regions are almost the same, and their amplitude and frequency are similar. On the millennial scale, three HS events can be clearly identified. All these show that the climate of the ASM region (EASM, ISM, and Central China) changes contemporaneously, within the age error range on the centennial and the millennial timescale. In addition, millennial and centennial variability both show an increasing trend since 19 kyr BP. This may be associated with the abnormally dry and cold HS1 event or deglaciation on the millennial–centennial time scales, which could be verified by long high-resolution records. On the suborbital time scale (**Figure 6B**), stalagmite $\delta^{18}O$ records in the three regions show three trends during the 24–16 kyr BP period. The Hulu Cave stalagmite $\delta^{18}O$ values in eastern China become gradually negative, consistent with the more positive nature of HS2, as compared to HS1. The Xiaobailong Cave $\delta^{18}O$ values from the ISM region gradually become more positive, while the DDH stalagmite $\delta^{18}O$ in Central China adopts an intermediate state between the EASM and ISM, further supporting the idea that the precipitation in Central China during the 24–19 kyr BP period was a mixture of water vapor from the Indian Ocean and the Pacific Ocean. This is probably caused by a decline in the sea level during the glacial period, while the ISM region was mainly influenced by ice volume (Cai et al., 2015; Xue et al., 2019). This difference on the orbital to sub-orbital timescale indicates that ASM rainfall isotope data also have regional differences, although precession is the main driver.

6 CONCLUSION

The DDH stalagmite $\delta^{18}O$ records from Shaanxi established by high-precision uranium dating have been used to reconstruct the Asian summer monsoon evolution history of 34–13 kyr BP. It is found that DDH stalagmite $\delta^{18}O$ records and those from other ASM regions are broadly consistent on orbital and millennial timescales. The DDH stalagmite $\delta^{18}O$ is controlled by low latitude summer insolation changes in the northern hemisphere on orbital timescale and responds to millennial climate changes from the northern high latitudes. Several cold HS events and DO climate cycles have been recorded. Spectrum analysis shows that the $\delta^{18}O$ of the DDH stalagmite has characteristic cycles of 500, 206, and 142 years, indicating that the ASM during the last glaical period is regulated in part by solar activity. Multi-scale EEMD decomposition shows that the stalagmite $\delta^{18}O$ in the three regions (ISM, EASM and Central China) changes consistently on millennial and centenary timescales, but there are also three characteristics for each region during the glacial period on the suborbital timescale, which is likely to be caused by changes in regional sea level differences. This underscores the important influence of water vapor sources on the Chinese stalagmite $\delta^{18}O$.

DATA AVAILABILITY STATEMENT

The raw data supporting the conclusion of this article will be made available by the authors, without undue reservation.

AUTHOR CONTRIBUTIONS

ZH supervised and managed the project. XC, YC and QC designed the research and experiments. XC, QC, GX, YC, QL, JZ, LT, YH, JR, PW, YW and YZ participated in field work and collected samples. XC, GX, HC and RE performed the experiments. XC, QC, YC, GX and JZ carried out data analysis. QC, XC and YC wrote and reviewed the manuscript.

FUNDING

This research was supported by the National Natural Science Foundation of China grants (41901096), the Strategic Priority Research Program of Chinese Academy of Sciences (Grant No. XDB 40010200), the Key R & D project of the Science and Technology Department of Shaanxi Province (2017ZDXM-SF-27-1), the Natural Science Foundation of Shaanxi Province general project (2020JQ-975), the Opening Fund of State Key Laboratory of Loess and Quaternary Geology (SKLLQG 1704 and SKLLQG 1803), the commonweal geological survey project of Shaanxi Province (202008, 201902, and 201916), and the National Natural Science Foundation of China grants (41888101).

ACKNOWLEDGMENTS

We acknowledge Le Ma for helping with the stable isotope measurements, Yanbin Lu and David Domínguez-Villar for reviewing the manuscript, George S. Burr for improving our English, and Yingying Wei and Jinhu Ren for the field work.

REFERENCES

Alley, R. B., Meese, D. A., Shuman, C. A., Gow, A. J., Taylor, K. C., Grootes, P. M., White, J. W. C., Ram, M., Waddington, E. D., Mayewski, P. A., and Zielinski, G. A. (1993). Abrupt Increase in Greenland Snow Accumulation at the End of the Younger Dryas Event. *Nature* 362 (6420), 527–529. doi:10.1038/362527a0

An, Z. (2000). The History and Variability of the East Asian Paleomonsoon Climate. *Quat. Sci. Rev.* 19 (1-5), 171–187. doi:10.1016/s0277-3791(99)00060-8

Baker, A., Ito, E., Smart, P. L., and McEwan, R. F. (1997). Elevated and Variable Values of ^{13}C in Speleothems in a British Cave System. *Chem. Geology.* 136 (3-4), 263–270. doi:10.1016/S0009-2541(96)00129-5

Bond, G. C., Showers, W., Elliot, M., Evans, M., Lotti, R., Hajdas, I., et al. (1999). The North Atlantic's 1-2 Kyr Climate Rhythm: Relation to Heinrich Events, Dansgaard/Oeschger Cycles and the Little Ice Age. *Geophys. Monograph-American Geophys. Union* 112, 35–58. doi:10.1029/gm112p0035

Cai, Y., An, Z., Cheng, H., Edwards, R. L., Kelly, M. J., Liu, W., et al. (2006). High-resolution Absolute-Dated Indian Monsoon Record between 53 and 36 Ka from Xiaobailong Cave, Southwestern China. *Geol* 34 (8), 621–624. doi:10.1130/G22567.1

Cai, Y., Fung, I. Y., Edwards, R. L., An, Z., Cheng, H., Lee, J.-E., et al. (2015). Variability of Stalagmite-Inferred Indian Monsoon Precipitation over the Past 252,000 Y. *Proc. Natl. Acad. Sci. U.S.A.* 112 (10), 2954–2959. doi:10.1073/pnas.1424035112

Cai, Y., Tan, L., Cheng, H., An, Z., Edwards, R. L., Kelly, M. J., et al. (2010). The Variation of Summer Monsoon Precipitation in central China since the Last Deglaciation. *Earth Planet. Sci. Lett.* 291 (1-4), 21–31. doi:10.1016/j.epsl.2009.12.039

Cai, Y., Zhang, M., Peng, Z., Lin, Y., An, Z., Zhang, Z., et al. (2001). The $\delta^{18}O$ Variation of a Stalagmite from Qixing Cave, Guizhou Province and Indicated Climate Change during the Holocene. *Chin.Sci.Bull.* 46 (22), 1904–1908. doi:10.1007/bf02901169

Chen, Q., Hong, Z., Luo, Q., Tang, L., Wang, P., Hu, Y., et al. (2020). Last Glacial Paleoclimate Record of Stalagmite Trace Elements from Didonghe Cave in Hanzhong. *J. Xi'an Univ. (Natural Sci. Edition)* 23 (3), 92–102.

Chen, S., Wang, Y., Cheng, H., Edwards, R. L., Wang, X., Kong, X., et al. (2016). Strong Coupling of Asian Monsoon and Antarctic Climates on Sub-orbital Timescales. *Sci. Rep.* 6 (1), 1–7. doi:10.1038/srep32995

Cheng, H., Edwards, R. L., Broecker, W. S., Denton, G. H., Kong, X., Wang, Y., et al. (2009). Ice Age Terminations. *science* 326 (5950), 248–252. doi:10.1126/science.1177840

Cheng, H., Edwards, R. L., Sinha, A., Spötl, C., Yi, L., Chen, S., et al. (2016). The Asian Monsoon over the Past 640,000 Years and Ice Age Terminations. *nature* 534 (7609), 640–646. doi:10.1038/nature18591

Cheng, H., Lawrence Edwards, R., Shen, C.-C., Polyak, V. J., Asmerom, Y., Woodhead, J., et al. (2013). Improvements in ^{230}Th Dating, ^{230}Th and 234U Half-Life Values, and U-Th Isotopic Measurements by Multi-Collector Inductively Coupled Plasma Mass Spectrometry. *Earth Planet. Sci. Lett.* 371-372, 82–91. doi:10.1016/j.epsl.2013.04.006

Cheng, H., Sinha, A., Wang, X., Cruz, F. W., and Edwards, R. L. (2012). The Global Paleomonsoon as Seen through Speleothem Records from Asia and the Americas. *Clim. Dyn.* 39 (5), 1045–1062. doi:10.1007/s00382-012-1363-7

Cheng, H., Zhang, H., Cai, Y., Shi, Z., Yi, L., Deng, C., et al. (2021). Orbital-scale Asian Summer Monsoon Variations: Paradox and Exploration. *Sci. China Earth Sci.* 64, 529–544. doi:10.1007/s11430-020-9720-y

Corrick, E. C., Drysdale, R. N., Hellstrom, J. C., Capron, E., Rasmussen, S. O., Zhang, X., et al. (2020). Synchronous Timing of Abrupt Climate Changes during the Last Glacial Period. *Science* 369 (6506), 963–969. doi:10.1126/science.aay5538

Dansgaard, W., Johnsen, S. J., Clausen, H. B., Dahl-Jensen, D., Gundestrup, N. S., Hammer, C. U., et al. (1993). Evidence for General Instability of Past Climate from a 250-kyr Ice-Core Record. *nature* 364 (6434), 218–220. doi:10.1038/364218a0

Ding, Z., Liu, T., Rutter, N. W., Yu, Z., Guo, Z., and Zhu, R. (1995). Ice-volume Forcing of East Asian winter Monsoon Variations in the Past 800,000 Years. *Quat. Res.* 44 (2), 149–159. doi:10.1006/qres.1995.1059

Dong, J., Shen, C.-C., Kong, X., Wang, Y., and Duan, F. (2018). Asian Monsoon Dynamics at Dansgaard/Oeschger Events 14-8 and Heinrich Events 5-4 in Northern China. *Quat. Geochronol.* 47, 72–80. doi:10.1016/j.quageo.2018.05.012

Dorale, J. A., Edwards, R., Ito, E., and González, L. (1998). Climate and Vegetation History of the Midcontinent from 75 to 25 ka: A Speleothem Record from Crevice Cave, Missouri, USA. *Science* 282 (5395), 1871–1874. doi:10.1126/science.282.5395.1871

Dorale, J. A., González, L. A., Reagan, M. K., Pickett, D. A., Murrell, M. T., and Baker, R. G. (1992). A High-Resolution Record of Holocene Climate Change in Speleothem Calcite from Cold Water Cave, Northeast Iowa. *Science* 258 (5088), 1626–1630. doi:10.1126/science.258.5088.1626

Dorale, J., and Liu, Z. (2009). Limitations of Hendy Test Criteria in Judging the Paleoclimatic Suitability of Speleothems and the Need for Replication. *J. cave karst Stud.* 71 (1), 73–80.

Duan, W., Cheng, H., Tan, M., and Edwards, R. L. (2016). Onset and Duration of Transitions into Greenland Interstadials 15.2 and 14 in Northern China Constrained by an Annually Laminated Stalagmite. *Sci. Rep.* 6 (1), 1–6. doi:10.1038/srep20844

Dutt, S., Gupta, A. K., Clemens, S. C., Cheng, H., Singh, R. K., Kathayat, G., et al. (2015). Abrupt Changes in Indian Summer Monsoon Strength during 33,800 to 5500 Years B.P. *Geophys. Res. Lett.* 42 (13), 5526–5532. doi:10.1002/2015GL064015

Dykoski, C. A., Edwards, R. L., Cheng, H., Yuan, D., Cai, Y., Zhang, M., et al. (2005). A High-Resolution, Absolute-Dated Holocene and Deglacial Asian Monsoon Record From Dongge Cave, China. *Earth & Planet. Sci. Lett.* 233 (1–2), 71–86. doi:10.1016/j.epsl.2005.01.036

Edwards, R. L., Chen, J. H., and Wasserburg, G. J. (1987). ^{238}U-^{234}U-^{230}Th-^{232}Th Systematics and the Precise Measurement of Time over the Past 500,000 Years. *Earth Planet. Sci. Lett.* 81 (2-3), 175–192. doi:10.1016/0012-821x(87)90154-3

Fairchild, I. J., Smith, C. L., Baker, A., Fuller, L., Spötl, C., Mattey, D., et al. (2006). Modification and Preservation of Environmental Signals in Speleothems. *Earth-Science Rev.* 75 (1-4), 105–153. doi:10.1016/j.earscirev.2005.08.003

Genty, D., Blamart, D., Ghaleb, B., Plagnes, V., Causse, C., Bakalowicz, M., et al. (2006). Timing and Dynamics of the Last Deglaciation From European and North African $\delta^{13}C$ Stalagmite Profiles-Comparison with Chinese and South Hemisphere Stalagmites. *Quat. Sci. Rev.* 25 (17–18), 2118–2142. doi:10.1016/j.quascirev.2006.01.030

Guo, Z., Biscaye, P., Wei, L., Chen, X., Peng, S., and Liu, T. (2000). Summer Monsoon Variations over the Last 1.2 Ma from the Weathering of Loess-Soil Sequences in China. *Geophys. Res. Lett.* 27 (12), 1751–1754. doi:10.1029/1999GL008419

Heinrich, H. (1988). Origin and Consequences of Cyclic Ice Rafting in the Northeast Atlantic Ocean during the Past 130,000 Years. *Quat. Res.* 29 (2), 142–152. doi:10.1016/0033-5894(88)90057-9

Hu, C., Henderson, G. M., Huang, J., Xie, S., Sun, Y., and Johnson, K. R. (2008). Quantification of Holocene Asian Monsoon Rainfall from Spatially Separated Cave Records. *Earth Planet. Sci. Lett.* 266 (3-4), 221–232. doi:10.1016/j.epsl.2007.10.015

Hu, J., Emile-Geay, J., Tabor, C., Nusbaumer, J., and Partin, J. (2019). Deciphering Oxygen Isotope Records from Chinese Speleothems with an Isotope-Enabled Climate Model. *Paleoceanography and Paleoclimatology* 34 (12), 2098–2112. doi:10.1029/2019PA003741

Hu, J., Lu, X., and Su, J. (2010). Analysis on Climatic Characteristics of Ningqiang County in Recent 51 Years. *J. Shaanxi Meteorology* 3, 18–21.

Jaffey, A. H., Flynn, K. F., Glendenin, L. E., Bentley, W. C., and Essling, A. M. (1971). Precision Measurement of Half-Lives and Specific Activities ofU235andU238. *Phys. Rev. C* 4 (5), 1889–1906. doi:10.1103/PhysRevC.4.1889

Jiang, X., He, Y., Shen, C.-C., Lee, S.-Y., Yang, B., Lin, K., et al. (2014). Decoupling of the East Asian Summer Monsoon and Indian Summer Monsoon between 20 and 17 Ka. *Quat. Res.* 82 (1), 146–153. doi:10.1016/j.yqres.2014.05.001

Johnsen, S. J., Clausen, H. B., Dansgaard, W., Fuhrer, K., Gundestrup, N., Hammer, C. U., et al. (1992). Irregular Glacial Interstadials Recorded in a New Greenland Ice Core. *Nature* 359 (6393), 311–313. doi:10.1038/359311a0

Kathayat, G., Cheng, H., Sinha, A., Spötl, C., Edwards, R. L., Zhang, H., et al. (2016). Indian Monsoon Variability on Millennial-Orbital Timescales. *Sci. Rep.* 6 (1), 1–7. doi:10.1038/srep24374

Lachniet, M. S. (2009). Climatic and Environmental Controls on Speleothem Oxygen-Isotope Values. *Quat. Sci. Rev.* 28 (5-6), 412–432. doi:10.1016/j.quascirev.2008.10.021

Li, D., Tan, L., Cai, Y., Jiang, X., Ma, L., Cheng, H., et al. (2019). Is Chinese Stalagmite $\delta^{18}O$ Solely Controlled by the Indian Summer Monsoon? *Clim. Dyn.* 53 (5), 2969–2983. doi:10.1007/s00382-019-04671-x

Li, T.-Y., Wu, Y., Shen, C.-C., Li, J.-Y., Chiang, H.-W., Lin, K., et al. (2021). High Precise Dating on the Variation of the Asian Summer Monsoon since 37 Ka BP. *Sci. Rep.* 11 (1), 1–14. doi:10.1038/s41598-021-88597-7

Li, Y., Rao, Z., Xu, Q., Zhang, S., Liu, X., Wang, Z., et al. (2020). Inter-relationship and Environmental Significance of Stalagmite $\delta^{13}C$ and $\delta^{18}O$ Records from Zhenzhu Cave, north China, over the Last 130 Ka. *Earth Planet. Sci. Lett.* 536, 116149. doi:10.1016/j.epsl.2020.116149

Liang, Y., Zhao, K., Edwards, R. L., Wang, Y., Shao, Q., Zhang, Z., et al. (2020). East Asian Monsoon Changes Early in the Last Deglaciation and Insights into the Interpretation of Oxygen Isotope Changes in the Chinese Stalagmite Record. *Quat. Sci. Rev.* 250, 106699. doi:10.1016/j.quascirev.2020.106699

Liu, D., Wang, Y., Cheng, H., Edwards, R. L., Kong, X., Chen, S., et al. (2018). Contrasting Patterns in Abrupt Asian Summer Monsoon Changes in the Last Glacial Period and the Holocene. *Paleoceanography and Paleoclimatology* 33 (2), 214–226. doi:10.1002/2017PA003294

Liu, G., Li, X., Chiang, H.-W., Cheng, H., Yuan, S., Chawchai, S., et al. (2020). On the Glacial-Interglacial Variability of the Asian Monsoon in Speleothem $\delta^{18}O$ Records. *Sci. Adv.* 6 (7), eaay8189. doi:10.1126/sciadv.aay8189

Liu, S., Liu, D., Wang, Y., Zou, L., and Gao, H. (2022). Spatio-temporal Expressions of Precessional-Scale Stalagmite $\delta^{18}O$ Variations from the Asian Monsoon Area. *Palaeogeogr. Palaeoclimatol. Palaeoecol.* 585, 110720. doi:10.1016/j.palaeo.2021.110720

Liu, Z., Wen, X., Brady, E. C., Otto-Bliesner, B., Yu, G., Lu, H., .Cheng, H., Wang, Y., Zheng, W., Ding, Y., Edwards, R. L., Cheng, J., Liu, W., and Yang, H. (2014). Chinese Cave Records and the East Asia Summer Monsoon. *Quat. Sci. Rev.* 83, 115–128. doi:10.1016/j.quascirev.2013.10.021

Lu, J., Zhang, H., Li, H., Sha, L., Zhao, J., Li, Y., et al. (2021). A 120-year Seasonally Resolved Speleothem Record of Precipitation Seasonality from southeastern China. *Quat. Sci. Rev.* 264, 107023. doi:10.1016/j.quascirev.2021.107023

Luo, Q., Zhang, J., Li, Y., Yin, Z., Tang, L., Wang, P., et al. (2019). Geologic Conditions and Distribution Features of Tiankeng Groups in Hanzhong, Shaanxi Province. *CARSOLOGICA SINICA* 38 (2), 281–291. doi:10.11932/karst20190214

MacAyeal, D. R. (1993). Binge/purge Oscillations of the Laurentide Ice Sheet as a Cause of the North Atlantic's Heinrich Events. *Paleoceanography* 8 (6), 775–784. doi:10.1029/93PA02200

Maher, B. A. (2008). Holocene Variability of the East Asian Summer Monsoon from Chinese Cave Records: a Re-assessment. *The Holocene* 18 (6), 861–866. doi:10.1177/0959683608095569

O'Neil, J. R., Clayton, R. N., and Mayeda, T. K. (1969). Oxygen Isotope Fractionation in Divalent Metal Carbonates. *J. Chem. Phys.* 51 (12), 5547–5558. doi:10.1063/1.1671982

Orland, I. J., Bar-Matthews, M., Kita, N. T., Ayalon, A., Matthews, A., and Valley, J. W. (2009). Climate Deterioration in the Eastern Mediterranean as Revealed by Ion Microprobe Analysis of a Speleothem that Grew from 2.2 to 0.9 Ka in Soreq Cave, Israel. *Quat. Res.* 71 (1), 27–35. doi:10.1016/j.yqres.2008.08.005

Pausata, F. S. R., Battisti, D. S., Nisancioglu, K. H., and Bitz, C. M. (2011). Chinese Stalagmite $\delta^{18}O$ Controlled by Changes in the Indian Monsoon during a Simulated Heinrich Event. *Nat. Geosci* 4 (7), 474–480. doi:10.1038/ngeo1169

Peterse, F., Martínez-García, A., Zhou, B., Beets, C. J., Prins, M. A., Zheng, H., et al. (2014). Molecular Records of continental Air Temperature and Monsoon Precipitation Variability in East Asia Spanning the Past 130,000 Years. *Quat. Sci. Rev.* 83, 76–82. doi:10.1016/j.quascirev.2013.11.001

Rasmussen, S. O., Bigler, M., Blockley, S. P., Blunier, T., Buchardt, S. L., Clausen, H. B., .Cvijanovic, I., Dahl-Jensen, D., Johnsen, S. J., Fischer, H., Gkinis, V., Guillevic, M., Hoek, W. Z., Lowe, J. J., Pedro, J. B., Popp, T., Seierstad, I. K., Steffensen, J. P., Svensson, A. M., Vallelonga, P., Vinther, B. M., Walker, M. J. C., Wheatley, J. J., and Winstrup, M. (2014). A Stratigraphic Framework for Abrupt Climatic Changes during the Last Glacial Period Based on Three Synchronized Greenland Ice-Core Records: Refining and Extending the INTIMATE Event Stratigraphy. *Quat. Sci. Rev.* 106, 14–28. doi:10.1016/j.quascirev.2014.09.007

Rohling, E., Liu, Q., Roberts, A., Stanford, J., Rasmussen, S., Langen, P., et al. (2009). Controls on the East Asian Monsoon during the Last Glacial Cycle, Based on Comparison between Hulu Cave and Polar Ice-Core Records. *Quat. Sci. Rev.* 28 (27-28), 3291–3302. doi:10.1016/j.quascirev.2009.09.007

Schulz, M., and Mudelsee, M. (2002). REDFIT: Estimating Red-Noise Spectra Directly from Unevenly Spaced Paleoclimatic Time Series. *Comput. Geosciences* 28 (3), 421–426. doi:10.1016/S0098-3004(01)00044-9

Shen, C., Edwards, R., Cheng, H., Dorale, J., Thomas, R., Moran, S., .and Edmonds, H. N. (2002). Uranium and Thorium Isotopic and Concentration Measurements by Magnetic Sector Inductively Coupled Plasma Mass Spectrometry. *Chem. Geology.* 185 (3-4), 165–178. doi:10.1016/S0009-2541(01)00404-1

Stuiver, M., and Braziunas, T. F. (1993). Sun, Ocean, Climate and Atmospheric $^{14}CO_2$: an Evaluation of Causal and Spectral Relationships. *The Holocene* 3 (4), 289–305. doi:10.1177/095968369300300401

Stuiver, M., Grootes, P. M., and Braziunas, T. F. (1995). The GISP2 $\delta^{18}O$ Climate Record of the Past 16,500 Years and the Role of the Sun, Ocean, and Volcanoes. *Quat. Res.* 44 (3), 341–354. doi:10.1006/qres.1995.1079

Tan, L., Cai, Y., Cheng, H., Edwards, L. R., Gao, Y., Xu, H., et al. (2018). Centennial- to Decadal-Scale Monsoon Precipitation Variations in the Upper Hanjiang River Region, China over the Past 6650 Years. *Earth Planet. Sci. Lett.* 482, 580–590. doi:10.1016/j.epsl.2017.11.044

Tan, L., Cai, Y., Cheng, H., Edwards, R. L., Shen, C. C., Gao, Y., et al. (2015). Climate Significance of Speleothem $\delta^{18}O$ from central China on Decadal Timescale. *J. Asian Earth Sci.* 106, 150–155. doi:10.1016/j.jseaes.2015.03.008

Tan, L., Cai, Y., Cheng, H., An, Z., and Edwards, R. L. (2009). Summer Monsoon Precipitation Variations in central China over the Past 750 Years Derived from a High-Resolution Absolute-Dated Stalagmite. *Palaeogeogr. Palaeoclimatol. Palaeoecol.* 280 (3-4), 432–439. doi:10.1016/j.palaeo.2009.06.030

Tan, M. (2014). Circulation Effect: Response of Precipitation $\delta^{18}O$ to the ENSO Cycle in Monsoon Regions of China. *Clim. Dyn.* 42 (3-4), 1067–1077. doi:10.1007/s00382-013-1732-x

Tierney, J. E., Poulsen, C. J., Montañez, I. P., Bhattacharya, T., Feng, R., Ford, H. L., .Hönisch, B., Inglis, G. N., Petersen, S. V., Sagoo, N., Tabor, C. R., Thirumalai, K., Zhu, J., Burls, N. J., Foster, G. L., Goddéris, Y., Huber, B. T., Ivany, L. C., Kirtland Turner, S., Lunt, D. J., McElwain, J. C., Mills, B. J. W., Otto-Bliesner, B. L., Ridgwell, A., and Zhang, Y. G. (2020). Past Climates Inform Our Future. *Science* 370 (6517). doi:10.1126/science.aay3701

Wang, B., and Ding, Q. (2008). Global Monsoon: Dominant Mode of Annual Variation in the Tropics. *Dyn. Atmospheres Oceans* 44 (3-4), 165–183. doi:10.1016/j.dynatmoce.2007.05.002

Wang, B., Wu, R., and Lau, K.-M. (2001a). Interannual Variability of the Asian Summer Monsoon: Contrasts between the Indian and the Western North Pacific-East Asian Monsoons*. *J. Clim.* 14 (20), 4073–4090. doi:10.1175/1520-0442(2001)014<4073:ivotas>2.0.co;2

Wang, P. X., Wang, B., Cheng, H., Fasullo, J., Guo, Z. T., Kiefer, T., et al. (2014). The Global Monsoon across Timescales: Coherent Variability of Regional Monsoons. *Clim. Past* 10 (6), 2007–2052. doi:10.5194/cp-10-2007-2014

Wang, Y., Cheng, H., Edwards, R. L., He, Y., Kong, X., An, Z., et al. (2005). The Holocene Asian Monsoon: Links to Solar Changes and North Atlantic Climate. *Science* 308 (5723), 854–857. doi:10.1126/science.1106296

Wang, Y., Cheng, H., Edwards, R. L., Kong, X., Shao, X., Chen, S., et al. (2008). Millennial- and Orbital-Scale Changes in the East Asian Monsoon over the Past 224,000 Years. *Nature* 451 (7182), 1090–1093. doi:10.1038/nature06692

Wang, Y. J., Cheng, H., Edwards, R. L., An, Z. S., Wu, J. Y., Shen, C.-C., et al. (2001b). A High-Resolution Absolute-Dated Late Pleistocene Monsoon Record from Hulu Cave, China. *Science* 294 (5550), 2345–2348. doi:10.1126/science.1064618

Wu, Y., Li, T.-Y., Yu, T.-L., Shen, C.-C., Chen, C.-J., Zhang, J., et al. (2020). Variation of the Asian Summer Monsoon since the Last Glacial-Interglacial Recorded in a Stalagmite from Southwest China. *Quat. Sci. Rev.* 234, 106261. doi:10.1016/j.quascirev.2020.106261

Wu, Z., and Huang, N. E. (2009). Ensemble Empirical Mode Decomposition: a Noise-Assisted Data Analysis Method. *Adv. Adapt. Data Anal.* 01 (01), 1–41. doi:10.1142/S1793536909000047

Xu, D., Lu, H., Chu, G., Liu, L., Shen, C., Li, F., et al. (2019). Synchronous 500-year Oscillations of Monsoon Climate and Human Activity in Northeast Asia. *Nat. Commun.* 10 (1), 1–10. doi:10.1038/s41467-019-12138-0

Xue, G., Cai, Y., Ma, L., Cheng, X., Cheng, H., Edwards, R. L., et al. (2019). A New Speleothem Record of the Penultimate Deglacial: Insights into Spatial Variability and Centennial-Scale Instabilities of East Asian Monsoon. *Quat. Sci. Rev.* 210, 113–124. doi:10.1016/j.quascirev.2019.02.023

Yuan, D., Cheng, H., Edwards, R. L., Dykoski, C. A., Kelly, M. J., Zhang, M., et al. (2004). Timing, Duration, and Transitions of the Last Interglacial Asian Monsoon. *Science* 304 (5670), 575–578. doi:10.1126/science.1091220

Zhang, H., Zhang, X., Cai, Y., Sinha, A., Spötl, C., Baker, J., et al. (2021). A Data-Model Comparison Pinpoints Holocene Spatiotemporal Pattern of East Asian Summer Monsoon. *Quat. Sci. Rev.* 261, 106911. doi:10.1016/j.quascirev.2021.106911

Zhang, Z., Li, G., Cai, Y., Cheng, X., Sun, Y., Zhao, J., et al. (2022). Millennial-Scale Monsoon Variability Modulated by Low-Latitude Insolation during the Last Glaciation. *Geophys. Res. Lett.* 49, e2021GL096773. doi:10.1029/2021GL096773

Zhao, J., Cheng, H., Yang, Y., Tan, L., Spötl, C., Ning, Y., et al. (2019). Reconstructing the Western Boundary Variability of the Western Pacific Subtropical High over the Past 200 Years via Chinese Cave Oxygen Isotope Records. *Clim. Dyn.* 52 (5), 3741–3757. doi:10.1007/s00382-018-4456-0

Zhu, Z., Feinberg, J. M., Xie, S., Bourne, M. D., Huang, C., Hu, C., et al. (2017). Holocene ENSO-Related Cyclic Storms Recorded by Magnetic Minerals in Speleothems of central China. *Proc. Natl. Acad. Sci. U.S.A.* 114 (5), 852–857. doi:10.1073/pnas.1610930114

Conflict of Interest: The authors declare that the research was conducted in the absence of any commercial or financial relationships that could be construed as a potential conflict of interest.

Publisher's Note: All claims expressed in this article are solely those of the authors and do not necessarily represent those of their affiliated organizations, or those of the publisher, the editors, and the reviewers. Any product that may be evaluated in this article, or claim that may be made by its manufacturer, is not guaranteed or endorsed by the publisher.